ACS OMEGA

http://pubs.acs.org/journal/acsodf

Article

Flame Temperature Measurement Based on Laser-Induced Breakdown Spectroscopy and Element Doping

Bin Tai, Xiaojian Hao,* Jia Wang, and Haoliang Sun

Cite This: *ACS Omega* 2021, 6, 27239−27246

Read Online

ACCESS | Metrics & More | Article Recommendations

ABSTRACT: In this study, based on the existing high-temperature measurement and calibration equipment, calibration experiments using the spectral emissivity of intrinsic element particles in the field were designed to achieve the accurate measurement of a temperature field. Laser-induced breakdown spectroscopy was used to select the corresponding elements, and the element doping method was used to approximate the real temperature field. After calibrating the camera, the temperature distribution and spectral emissivity distribution of the flame were calculated. The range of calculated values was determined to be well-consistent with data collected using an infrared thermal imager, which verified the accuracy of the experiment.

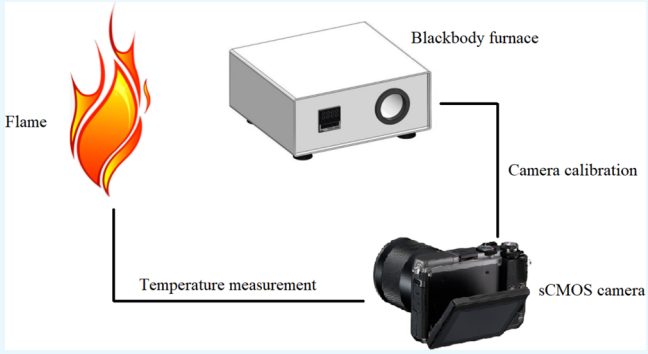

1. INTRODUCTION

Owing to the influence of an extreme environment such as high temperature, pressure, speed, and impact, it is difficult to accurately measure the transient high temperature of an intense flame at the scene of an explosion. This kind of transient temperature measurement is often accompanied by high-pressure or high-speed air flow, most of which are nonrepeatable one-time processes. Therefore, poor measurement conditions, high technical difficulty, and inaccurate temperature measurement are problems that cannot be ignored. At the same time, system reliability and data acquisition speed also put forward high requirements. The combustion of a fireball includes various physical phenomena, such as fluid flow, fluid heat transfer, and chemical reaction. Although many temperature sensors are suitable for different temperature ranges and response speeds, theoretical research and the practice of temperature measurement remain insufficient.

Owing to their low cost, direct temperature measurement principle, and high reliability of measurement, high-temperature thermocouples, as the most common contact temperature sensor, are widely used in the measurement of complex temperature fields. However, owing to their invasive nature and limited response speed, it is difficult to reflect the complete distribution of a temperature field only through multipoint measurements. Many scientific research institutions have gathered numerous research results for the contact measurements of the high-temperature fields of explosions.[1−5] Owing to its significant disturbance of the temperature field, a thermocouple mostly plays a role in verifying the noncontact measurements of a flame temperature field.[6−8] Compared with the contact temperature measurement method, the noncontact temperature measurement method has the advantages of minimal temperature field disturbance, fast response speed, and wide measurement range. For example, Shuai and others designed an ultrasonic guided wave thermometer and conducted high-temperature measurements.[9] Qi of Tsinghua University and others used transverse shear interferometry to measure and visualize the temperature field of a symmetrical, annular, ethylene laminar-diffusion flame and performed algebraic inversion calculations of its refractive index.[10] The peak temperature of the flame can reach 1980−2440 K. The California State University Banks' team used planar laser-induced fluorescence to build a measurement system to measure the bubble temperature of laser-induced cavitation.[11] According to the unique optical characteristics of the medium in the temperature field and their influence on the optical transmission process, the team from Sungkyunkwan University in Korea combined tunable semiconductor laser absorption spectroscopy (TDLAS) and laser-induced breakdown spectroscopy (LIBS) technology to analyze the optical absorption and emission characteristics of medium particles in a flame temperature field. Thus, a flame radial temperature distribution and gas molecular absorption coefficient distribution were

Received: July 27, 2021
Accepted: September 20, 2021
Published: October 6, 2021

https://doi.org/10.1021/acsomega.1c04025
ACS Omega 2021, 6, 27239−27246

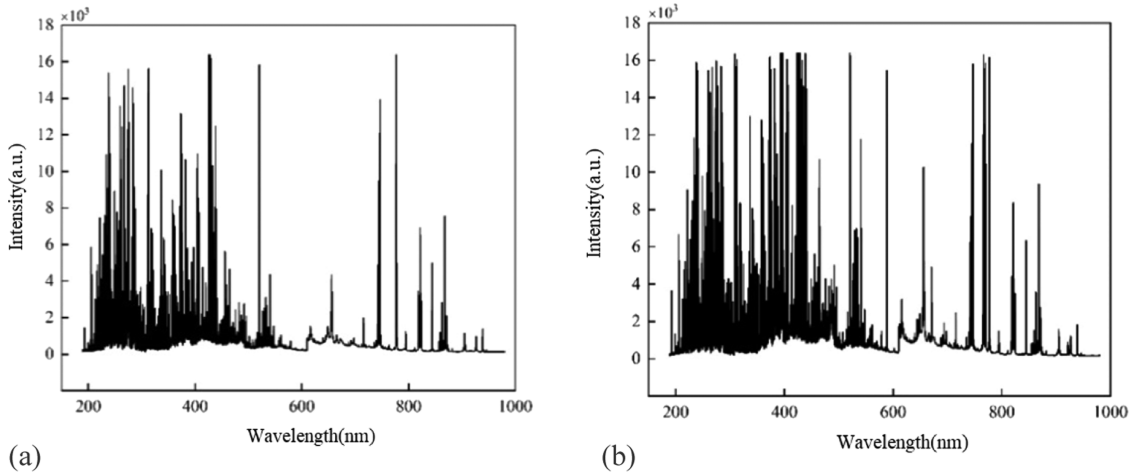

Figure 1. Energy spectrum analysis. (a) Average energy spectrum of the stainless-steel substrate and (b) average energy spectrum of the black powder residue.

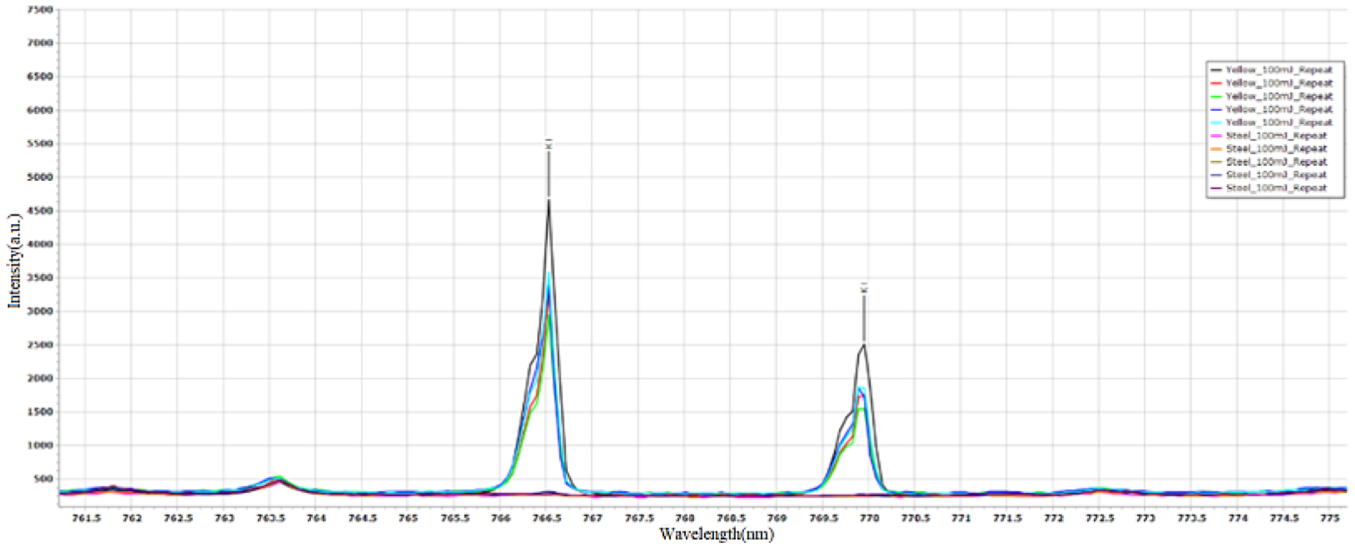

Figure 2. Characteristic energy spectra of K (766.60 and 769.90 nm).

obtained via TDLAS, and the variation law of molecular concentration under different equivalence ratios was explored via LIBS.[12] Professor Ghezelbash's team from Malek Ashtar University of Technology in Iran used LIBS to analyze the temperature field of different types of laminar diffusion flames; they divided the flame area according to height information and obtained the excitation spectral properties of characteristic elements and groups in different areas of the flame.[13] With regard to the thermal and optical radiation emission of medium particles in the temperature field, Professor Zhou et al. conducted a detailed analysis combining spectral analysis and radiation temperature measurement technology. According to the overall spectral characteristics of the flame temperature field, strong emission lines of alkali metal elements were reasonably avoided, and the radiation transfer model was simplified. However, it is difficult to determine the flame emissivity when it changes with wavelength. Combined with the colorimetric temperature measurement method, the two-dimensional spectral emissivity and temperature field of the flame in a pulverized coal combustion furnace were determined.[14]

All of the abovementioned temperature measurement methods have their unique advantages and specific applications, but they also have certain limitations because of their own service conditions and equipment dependence, resulting in problems such as difficulty in application for field-test experiments, excessively expensive equipment, and high actual test costs. Therefore, based on the research of various measurement methods, this study aims to integrate the advantages of various methods and select appropriate temperature measurement methods for combining and optimizing various methods. In this article, we have designed a new flame temperature measurement method. Through the combination of LIBS and element doping, data calibration using a camera and doping particles was conducted using a standard blackbody furnace, and the functional relationship between the corresponding gray values and temperature, as well as the functional relationship between the spectral radiance and the emissivity of the doping elements, was fitted. The distribution range of the flame was obtained by calculating the functional relationship obtained by fitting. The flame temperature was determined with an infrared thermal imager, and the

https://doi.org/10.1021/acsomega.1c04025
ACS Omega 2021, 6, 27239−27246

experimental results were in good agreement with the calculated results.

2. THEORETICAL BACKGROUND AND ELEMENT ANALYSIS

Radiation refers to the phenomenon where part of the electromagnetic energy emitted by a field source propagates away from and then does not return to the source. The energy diffuses outward in the form of electromagnetic waves or particles. The medium in the temperature field is excited by local high heat in a high-temperature environment, and the particles in the medium change from the ground state to the excited state. When the dielectric particles in the ground state inside the temperature field are excited by local high heat, a transition from the ground state to the excited state will occur, and excited atoms or ions will be generated. Then, the energy-level transition from the high-energy state to the low-energy state will occur within 10−8 s, and optical radiation with its own characteristics will be emitted to release energy outside the system in the form of light. It is difficult to accurately measure the temperature field due to the interference of various substances and the influence of the extreme environment. Therefore, it is necessary to analyze the specific medium in the temperature field to measure the temperature.

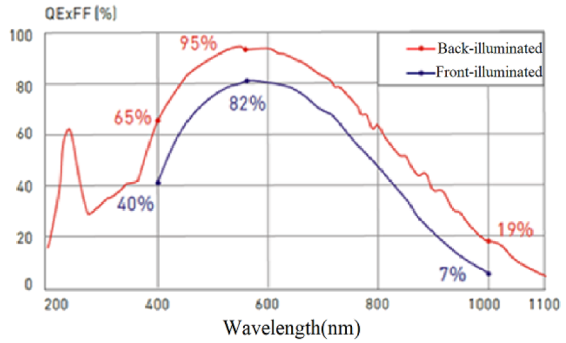

Figure 3. sCMOS quantum efficiency curve.

Table 1. sCMOS Camera Parameters

parameter	DHYANA 400BSI
sensor size	1.2″
sensor type	back-illuminated sCMOS
number of effective pixels	2048 (H) × 2048 (V)
single pixel size	6.5 μm × 6.5 μm
frame rate	74 fps@4.2 MP
time of exposure	6.6 μs to 10 s

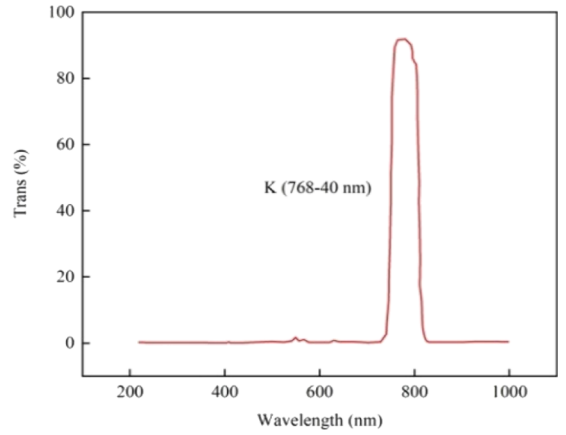

Figure 4. Transmission characteristic curve of the K element filter.

Based on the excitation effect of intrinsic element energy spectra in high-temperature fields, it is necessary to study the radiation intensity of the specific internal material excited by heating and establish the corresponding relationship between the radiance L and node temperature T. According to Planck's blackbody radiation law, we can first determine the relationship between spectral radiance and temperature in a blackbody environment

$$\begin{cases} L_b(\lambda, T_b)\,\mathrm{d}\lambda = \dfrac{c_1}{\pi}\cdot\lambda^{-5}(\mathrm{e}^{c_2/\lambda T_b} - 1)^{-1}\,\mathrm{d}\lambda \\ c_1 = 3.741771852 \times 10^{-16}\ (\mathrm{W\cdot m^2}) \\ c_2 = 1.438776877 \times 10^{-2}\ (\mathrm{m\cdot K}) \end{cases} \quad (1)$$

where $L_b(\lambda, T)$ is the spectral radiance of an ideal blackbody; T_b is the ideal blackbody temperature at wavelength λ; and c_1 and c_2 are the first and second radiation constants, respectively.

For a real object, its emissivity cannot reach 0.99 of the blackbody. Therefore, based on Planck's blackbody radiation law, the thermal and optical radiation of a real object needs to be calculated using its spectral emissivity

$$L(\lambda, T) = L_b(\lambda, T)\cdot\varepsilon(\lambda, T) \quad (2)$$

where $L(\lambda, T)$ is the spectral radiance of the real object; T is the blackbody temperature at wavelength λ; and $\varepsilon(\lambda, T)$ is the spectral emissivity of the real object.

To measure the radiance of an actual object, we must first calculate its emissivity. Since we cannot directly obtain the relationship between the gray value and blackbody temperature, the gray value and radiance, and the emissivity and blackbody temperature to complete the modeling of thermo-optical coupling in the temperature measurement process, we need to calibrate a camera to obtain the relationship between the gray value and the blackbody temperature.

Usually at a high-temperature explosion site, potassium (K) will be in the temperature field. Therefore, we decided to use K as our doped element.[15]

To increase the reliability of determining elements in the experiment, we chose black powder as our experimental object and used a laser to strike its combustion residue via LIBS to analyze its internal element composition and spectral information. To clearly observe the spectral curve of the combustion residues of energetic materials, we used blank stainless steel as the substrate for data analysis. Figure 1 shows the average energy spectra of the combustion residues of the stainless-steel substrate and black powder.

After observing their spectral differences, it was found that compared to the stainless-steel substrate, the black powder combustion residue had additional characteristic peaks at various wavelengths. Combined with the National Institute of National Institute of Standards and Technology (NIST) spectral database for further element determination, K exhibited strong spectral line peaks at 766.60 and 769.90 nm, as shown in Figure 2. This experiment also confirmed that K could competently serve as a doping element when measuring the temperature field.

The camera used for calibration was a Tucsen Photonics Dhyana 400bsi ultrahigh sensitivity sCMOS scientific camera,

https://doi.org/10.1021/acsomega.1c04025
ACS Omega 2021, 6, 27239−27246

and its quantum efficiency is shown in Figure 3. The parameters of the camera are shown in Table 1.

As mentioned above, K was used as the dopant for our temperature measurements. To measure the spectral information of K, a 768 nm filter was installed in front of the camera lens. The transmission characteristics of the K filter are shown in Figure 4.

Combining the characteristic energy spectrum of K, the transmission characteristics of the filter, and the quantum efficiency of the camera, the camera was found to have a high quantum efficiency in the band of 766.6−769.9 nm.

Since there is no elemental form of K in nature, we selected potassium sulfate (K_2SO_4) as our doping element in light of its physicochemical properties and abundant NIST library data.

3. CAMERA CALIBRATION

We defined the blackbody radiation source area as A_c, the entrance pupil area of the instrument to be calibrated as A_p,

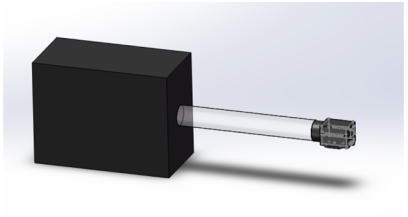

Figure 5. Calibration diagram.

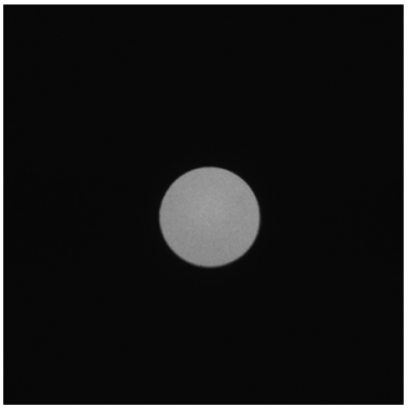

Figure 6. Gray image of a medium-temperature blackbody furnace.

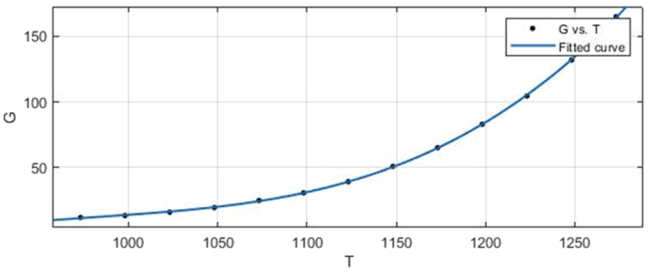

Figure 7. Blackbody temperature and imaging gray value.

and the effective photosensitive area of the pixel plane of the detection module as A_s. The effective emissivity ε of the blackbody furnace cavity can be expressed as follows

$$\varepsilon = \frac{\varepsilon_0[1 + (1 - \varepsilon_0)(\Delta S/S - \Delta\Omega/\pi)]}{\varepsilon_0(1 - \Delta S/S) + \Delta S/S} \tag{3}$$

where ε_0 and S are the emissivity and area (including opening area) of the inner wall material of the blackbody cavity, respectively; ΔS is the opening area; and $\Delta\Omega$ is the solid angle of the cavity corresponding to the opening of the blackbody cavity. The thermal radiation power emitted by the microfacet on the blackbody (small area) source to the solid angle of the optical module through the optical aperture D is as follows

$$d\Phi = \pi L_t \, dA_c \sin^2 u_0 \tag{4}$$

After passing through an optical lens with a transmission ratio of τ_{lens}, the radiation power transmitted to the pixel plane of the instrument to be calibrated is as follows

$$d\Phi = \pi\tau_{lens} L_t \, dA_c \sin^2 u_0 \tag{5}$$

Since the media on both sides of the optical lens remained unchanged, we can see that the refractive index on both sides is $n_0 = n_1$. Based on the Lagrange invariant (6) of the coaxial spherical system, the abovementioned formula can be rewritten as eqs 7 and 8

$$n_0 \cdot r_{A_c} \cdot \sin u_0 = n_1 \cdot r_{A_s} \cdot \sin u_1 \tag{6}$$

$$d\Phi = \pi\tau_{lens} L_t \, dA_c \sin^2 u_1 \tag{7}$$

$$d\Phi = L_t \cdot \frac{\pi\tau_{lens}}{1 + \frac{1}{4}\left(\frac{D}{f'}\right)^2} dA_c = L_t \cdot \frac{\pi D^2 l^2 \tau_{lens}}{4\left(l^2 + \left(\frac{D}{2}\right)^2\right)} d\Omega \approx L_t \cdot \frac{\pi D^2 \tau_{lens}}{4} d\Omega \tag{8}$$

where D is the optical aperture of the optical component of the instrument to be calibrated; $dA_c = dA_s$ is the microelement area of the black surface; L_t is the comprehensive radiance considering all kinds of external attenuation; and $d\Omega = \frac{dA_s}{f'^2}$ is the space solid angle corresponding to the selected single pixel.

Therefore, according to the fixed transformation relationship between the thermal radiation flux and the thermal radiation illuminance, the thermal light radiation illuminance received by the central pixel area of the pixel plane can be obtained as follows

$$E = \frac{d\Phi}{dA_s} \tag{9}$$

$$E = L_t \cdot \frac{\pi D^2 \tau_{lens}}{4f'^2} = L_t \cdot \frac{\pi}{4} \cdot \tau_{lens} \cdot \left(\frac{D}{f'}\right)^2 = L_t \cdot \frac{\pi}{4} \cdot \tau_{lens} \cdot D'^2 \tag{10}$$

where D' is the relative aperture of the optical component.

The thermal radiation transmitted to the optical lens of the detection module was attenuated by the atmospheric environment and the attenuator into different degrees and contains the background radiation and other interference radiation of the environment. Assuming that the radiator is a Lambert radiation source, that is, its spectral radiance is the same in all directions, the integrated radiance transmitted to the optical lens area of the instrument to be calibrated is as follows

$$L_t(\lambda, T) = \varepsilon \cdot \tau_{air} \cdot \tau_{redc} \cdot (L_{bs}(\lambda, T_t) + (1 - \varepsilon)\varepsilon_e L_b(\lambda, T_{env})) \tag{11}$$

https://doi.org/10.1021/acsomega.1c04025
ACS Omega 2021, 6, 27239−27246

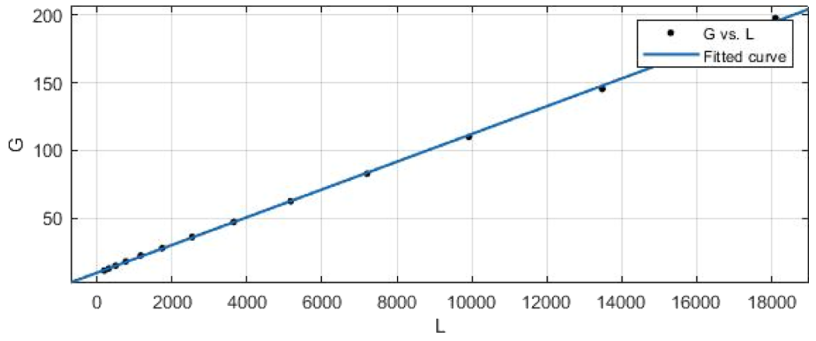

Figure 8. Imaging gray value and blackbody spectral radiance.

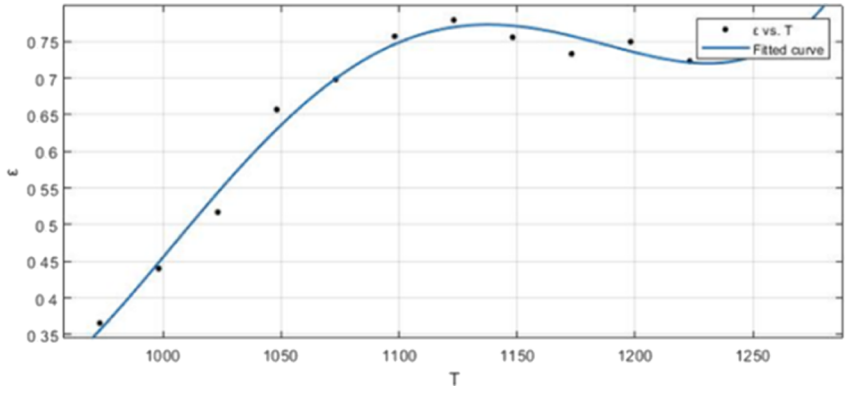

Figure 9. Emissivity of K and temperature of the blackbody furnace.

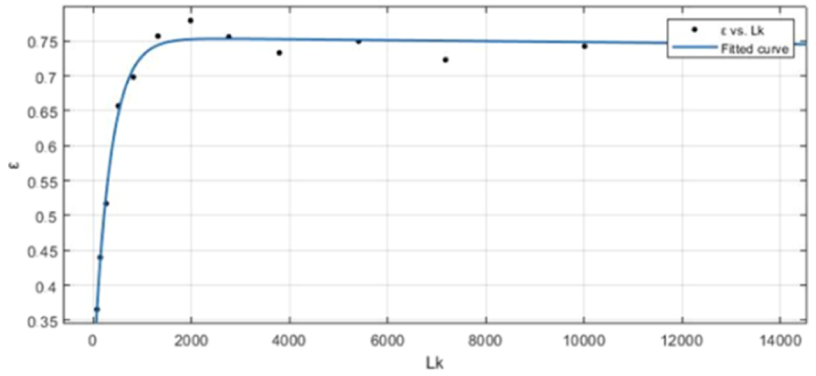

Figure 10. Emissivity and spectral radiance of the K element.

According to the equivalent transformation relationship between the small blackbody and surface radiation source

$$L_{bs} = L_b \frac{A_c}{A_p} = L_b \frac{4A_c}{\pi D^2} \tag{12}$$

The results are as follows

$$L_t(\lambda, T) = \varepsilon \cdot \tau_{air} \cdot \tau_{redc} \cdot \left(\frac{4A_c}{\pi D^2} L_b(\lambda, T_t) + (1 - \varepsilon) \varepsilon_e L_b(\lambda, T_{env}) \right) \tag{13}$$

where ε is the effective spectral emissivity of the equivalent blackbody radiation source; τ_{air}, τ_{redc}, and τ_{lens} are the spectral transmittance of the atmospheric environment, attenuator, and optical components, respectively; and ε_e is the spectral emissivity of the external atmospheric environment.

For a multichannel instrument, the output gray response signal of each channel in the working band can be expressed as

$$G_{ib}(\lambda) = g \cdot t_{int} \cdot \int_{\lambda_1}^{\lambda_2} E(\lambda, T) \cdot R_i(\lambda)\, d\lambda + G_{ip} \tag{14}$$

where g is the corresponding voltage gain of the detection module; t_{int} is the exposure (integration) time of the detection module camera; $E(\lambda, T)$ is the irradiance of a single pixel in channel i of the detection module; $R_i(\lambda)$ is the spectral responsivity of the i channel of the detection module, where the average value of the selected bandwidth band can be taken; and G_{ip} is the gray offset generated at the pixel, which can be expressed by the gray response value of the detection module when there is no radiance input.

Because the integral term in eq 14 is continuous for $[\lambda_1, \lambda_2]$, according to the integral mean value theorem, it can be

https://doi.org/10.1021/acsomega.1c04025
ACS Omega 2021, 6, 27239−27246

concluded that there is at least one $[\lambda_1, \lambda_2]$ in the filter bandwidth interval ξ

$$G_{ib}(\lambda) = (\lambda_2 - \lambda_1)\cdot R_i(\xi)\cdot L_t(\xi, T) + G_{ip} \quad (15)$$

The abovementioned formula can be expressed as

$$G_{ib}(\lambda) = A_i L_t(\lambda, T) + B_i \quad (16)$$

where $L(\xi, T)$ is the spectral radiance of the channel at a certain temperature at a specific wavelength ξ, and ξ can take the wavelength median of the selected bandwidth band; A_i is the linear coefficient of channel i of the detection module and can be regarded as a constant coefficient when the basic parameters of the detection module are unchanged; and B_i is the gray response offset. Given the filter and the module to be calibrated, the relationship between the comprehensive radiance L_t and the average gray response signal G_{ib} of the instrument can be obtained. Furthermore, the linear function relationship between the ideal surface radiation source temperature T and the average response signal G_{ib} can be obtained according to Planck's law.

The camera calibration used a medium-temperature blackbody furnace in the range of 0−1400 K. The blackbody chamber had an inner diameter of 25.4 mm, a length of 100 mm, and a spectral emissivity of approximately 0.99. The experiment was conducted in a dark room to reduce the interference of background light. Before the experiment, the camera was fixed at 0.5 m away from the blackbody furnace. During the experiment, the measurement was conducted every 50 K, and 40 frames of gray images were collected each time. Considering that the radiation of the central point of blackbody radiation is usually different from that of the surrounding positions, to solve the problem of blackbody radiation nonuniformity, we batch-processed the grayscale images at each temperature after image acquisition. The feature-extraction method based on gray histograms was used to threshold-segment the calibrated image, extract the luminous-effective part of the blackbody cavity, average the gray value in the region, and finally fit the temperature value and the average gray value. The relationship between spectral radiance and average gray value was obtained by Planck's law (Figure 5).

At the end of the experiment, the collected images were processed in batches, and the relationship between the blackbody temperature and the imaging gray value was fitted according to the gray value data and temperature data (Figures 6 and 7)

$$G_\lambda(T) = 1.165 \times 10^{-5} T_b^{\,3} - 0.03635 T_b^{\,2} + 37.92 T_b - 1.32 \times 10^4 \quad (17)$$

where $G_\lambda(T)$ is the gray value of the blackbody image collected by the camera and T_b is the temperature value of the blackbody.

According to formula 17, we can calculate the spectral radiance of the blackbody environment at different temperatures and then fit the relationship between the imaging gray value and the spectral radiance according to the gray value data and the spectral radiance data (Figure 8)

$$G_\lambda(T) = 0.01015 L_b(T) + 11.04 \quad (18)$$

where $L_b(T)$ is the spectral radiance in the blackbody environment.

Because the radiation of K was not as strong as that of the blackbody, the ratio of spectral radiance of K to that of the blackbody at the same temperature equaled the emissivity of K

$$\varepsilon = \frac{L_\varepsilon(\lambda, T)}{L_b(\lambda, T)} \quad (19)$$

According to the formula, to obtain the emissivity of K, its spectral radiance must be determined (Figures 9 and 10). According to the previous steps of analysis and calculation, the relationship between the emissivity of K, the temperature of the blackbody furnace, and the spectral radiance of the blackbody is obtained

$$\begin{cases} \varepsilon = 0.7551 \times \exp(-9.153 \times 10^{-7} L_\varepsilon) - 0.4799 \times \exp(-0.002924 L_\varepsilon) \\ \varepsilon = 3.71 \times 10^{-10} T^4 - 1.626 \times 10^{-6} T^3 + 0.002654 T^2 - 1.909 T + 511 \end{cases} \quad (20)$$

where ε is the spectral emissivity of K element, L_ε is the spectral radiance of K element at the corresponding temperature, and T is the current temperature value.

4. EXPERIMENT AND RESULT ANALYSIS

Ethane (C_2H_6) was used in the experiment as a fuel source. To meet the calibration range of the medium-temperature blackbody furnace, after turning on the Bunsen lamp, the air inlet of a Bunsen lamp was adjusted to ensure that the temperature was within the calibration range using a thermocouple. When the flame was burning, a powder feeder was used to evenly disperse K_2SO_4 powder into the flame. The previous camera calibration equipment remained unchanged, and multiple groups of gray images were collected. The

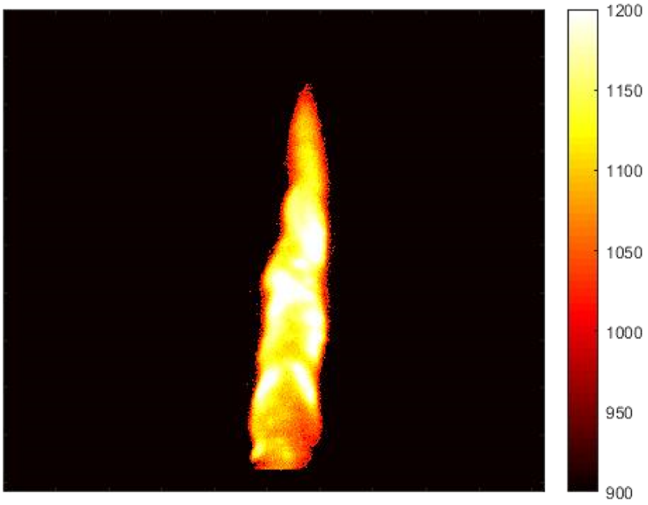

Figure 11. Calculation chart of flame temperature.

Table 2. Infrared Thermal Imager Parameters

measuring range	−40 to 2000 °C
emissivity range	0.1−1
detection band	8−14 μm
sensor	CMOS
resolving power	640 × 480
frame rate	50−60 Hz

https://doi.org/10.1021/acsomega.1c04025
ACS Omega 2021, 6, 27239−27246

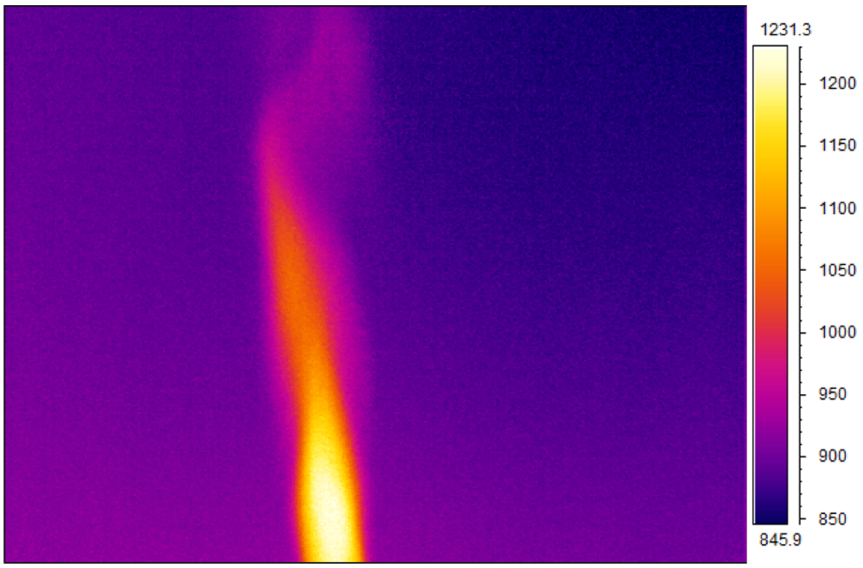

Figure 12. Infrared acquisition chart of flame temperature.

temperature was calculated via the fitting formula in the previous section. The temperature results are shown in Figure 11.

To verify the calculated results, a DL700 infrared thermal imager from Dali Science and Technology Co. was used in the experiment. The parameters of the infrared thermal imager are shown in Table 2.

Combined with the analysis and conclusions of infrared emissivity of several gas flames evaluated by Yuen,[16] the average infrared spectral emissivity of the flame was approximately 0.19 after several temperature measurements and comprehensive analyses of the flame at different heights. The standard temperature range measured using the infrared thermal imager was 845.9−1231.3 K, which was close to the calculated result obtained using the element doping method, as shown in Figure 11. Thus, the feasibility of the intrinsic element doping method for measuring a temperature field was verified experimentally (Figure 12).

5. RESULTS AND DISCUSSION

This study creatively proposed an element doping method to measure a temperature field. According to experimental temperature field requirements, LIBS spectrum analysis experiments were conducted to analyze the characteristic energy spectrum of elements in black powder, and K was selected as a doping element. A calibration experiment of the spectral emissivity of intrinsic element particles in the temperature field was designed. The relationship between the correlation temperature and gray value, the spectral radiance, and the emissivity of the doped elements was obtained. The temperature range of the flame was further determined by fitting the function relationship between emissivity and temperature, which was verified using an infrared thermal imager. The range of the calculated value well-matched the data collected using the infrared thermal imager, which verified the feasibility of the element doping method proposed in this study. This method provided a new scheme for the measurement of flame temperature fields, which can be applied to the measurement of temperature fields in more complex and extreme environments.

AUTHOR INFORMATION

Corresponding Author

Xiaojian Hao − *Science and Technology on Electronic Test and Measurement Laboratory, North University of China, Taiyuan, Shanxi Province 030051, China; School of Instrument and Electronics, North University of China, Taiyuan 030051, China; Shanxi Key Laboratory of Signal Capturing & Processing, North University of China, Taiyuan, Shanxi Province 030051, China*; Email: s1906155@st.nuc.edu.cn

Authors

Bin Tai − *Science and Technology on Electronic Test and Measurement Laboratory, North University of China, Taiyuan, Shanxi Province 030051, China; School of Instrument and Electronics, North University of China, Taiyuan 030051, China; Shanxi Key Laboratory of Signal Capturing & Processing, North University of China, Taiyuan, Shanxi Province 030051, China*; orcid.org/0000-0003-2227-6297

Jia Wang − *Science and Technology on Electronic Test and Measurement Laboratory, North University of China, Taiyuan, Shanxi Province 030051, China; School of Instrument and Electronics, North University of China, Taiyuan 030051, China; Shanxi Key Laboratory of Signal Capturing & Processing, North University of China, Taiyuan, Shanxi Province 030051, China*

Haoliang Sun − *Science and Technology on Electronic Test and Measurement Laboratory, North University of China, Taiyuan, Shanxi Province 030051, China; School of Instrument and Electronics, North University of China, Taiyuan 030051, China*

Complete contact information is available at: https://pubs.acs.org/10.1021/acsomega.1c04025

Notes

The authors declare no competing financial interest.

ACKNOWLEDGMENTS

This work was supported by the National Natural Science Foundation of China (NSFC) (nos. 52075504, 51575499, and

61473267), Pre-Research Field Foundation of Equipment Development Department of China (no. 61400030201), Pre-Research Key laboratory Foundation of Equipment Development Department of China (no. 6142001190413), the Open Fund of State Key Laboratory of Deep Buried Target Damage (no. DXMBJJ2018-09), Fund for Shanxi "1331Project" Key Subject Construction, and Fund for Shanxi Key Laboratory of Signal Capturing & Processing (no. ISPT2020-10). We thank LetPub (www.letpub.com) for its linguistic assistance during the preparation of this manuscript.

REFERENCES

(1) Zhang, R. *Research on Explosion Transient Temperature Measurement*; North University of China, 2013.
(2) Wang, D.; Song, L.; Zhang, Z. Contact Measuring Method of Explosion Temperature Based on Tungsten-rhenium Thermocouple. *J. Detect. Control* **2012**, *034*, 23−28.
(3) Tao, J.; Deren, K.; Yuyan, G. Design of a new type of an infrared heat flux density sensor. *Foreign Electron. Meas. Technol.* **2017**, *36*, 38−42.
(4) Li, Z.; Wang, S.; Gou, B. Study on Temperature Measurement in Closed Explosion Space. *Initiators Pyrotech.* **2012**, *5*, 52−56.
(5) Ji, J.; Su, J.; Li, Z.; Wang, G. Analysis of Hot Response of WRe5/26 Thermocouple to Explosive Products. *Chin. J. Explos. Propellants* **2008**, *31*, 26−29.
(6) Hossain, M. M.; Lu, G.; Sun, D.; Yan, Y. Three-dimensional reconstruction of flame temperature and emissivity distribution using optical tomographic and two-colour pyrometric techniques. *Meas. Sci. Technol.* **2013**, *24*, 074010.
(7) Ma, B.; Wang, G.; Magnotti, G.; Barlow, R. S.; Long, M. B. Intensity-ratio and color-ratio thin-filament pyrometry: Uncertainties and accuracy. *Combust. Flame* **2014**, *161*, 908−916.
(8) Gerasyutenko, V. V.; Sharkov, A. V.; Korablev, V. A.; Minkin, D. A. Improvement of Methods and Means for the Verification and Calibration of Thermal Imagers. *Meas. Tech.* **2020**, *63*, 455−462.
(9) Shuai, L. *Design of Micro Ultrasonic Guide Temperature Measurement*; North University of China, 2018.
(10) Qi, C.; Zheng, S.; Zhou, H. Experimental investigation on gas-phase temperature of axisymmetric ethylene flames by large lateral shearing interferometry. *Int. J. Therm. Sci.* **2017**, *115*, 104−111.
(11) Banks, D.; Robles, V.; Zhang, B.; Devia-Cruz, L. F.; Camacho-Lopez, S.; Aguilar, G. Planar laser induced fluorescence for temperature measurement of optical thermocavitation. *Exp. Therm. Fluid Sci.* **2019**, *103*, 385−393.
(12) Lee, J.; Bong, C.; Yoo, J.; Bak, M. S. Combined use of TDLAS and LIBS for reconstruction of temperature and concentration fields. *Opt. Express* **2020**, *28*, 21121−21133.
(13) Ghezelbash, M.; Majd, A. E.; Darbani, S. M. R.; Mousavi, S. J.; Ghasemi, A.; Tehrani, M. K. Spatial investigation of plasma emission from laminar diffusion methanol, ethanol, and n-propanol alcohol flames using LIBS method. *Appl. Phys. B: Lasers Opt.* **2017**, *123*, 36.
(14) Yan, W.; Zhou, H.; Jiang, Z.; Lou, C.; Zhang, X.; Chen, D. Experiments on Measurement of Temperature and Emissivity of Municipal Solid Waste (MSW) Combustion by Spectral Analysis and Image Processing in Visible Spectrum. *Energy Fuels* **2013**, *27*, 6754−6762.
(15) Sun, Z.-W.; Zhang, G.-N.; Qiao, T.; Llu, Z.-F.; Wang, P.; Zhu, J. Research progress of explosive post-blast residue analysis. *Chem. Res. Appl.* **2020**, *32*, 1117−1125.
(16) Yuen, W. W.; Tien, C. L. A simple calculation scheme for the luminous-flame emissivity. *Symp. Combust.* **1977**, *16*, 1481−1487.

https://doi.org/10.1021/acsomega.1c04025
ACS Omega 2021, 6, 27239−27246